Ceramics International 50 (2024) 819–828

Contents lists available at ScienceDirect

Ceramics International

journal homepage: www.elsevier.com/locate/ceramint

New trifunctional acrylic water-based paint with self-cleaning, biocidal and magnetic properties

Izabela Malinowska [a], Oliwia Paszkiewicz [b], Agata Markowska-Szczupak [b], Anna Zielińska-Jurek [a,*]

[a] Department of Process Engineering and Chemical Technology, Faculty of Chemistry, Gdansk University of Technology, Narutowicza 11/12, 80-233, Gdansk, Poland
[b] Department of Chemical and Process Engineering, West Pomeranian University of Technology in Szczecin, Al. Piastów 42, 71-065, Szczecin, Poland

ARTICLE INFO

Handling Editor: Dr P. Vincenzini

Keywords:
Self-cleaning paint
Magnetic paint
Biocidal paint
Photocatalytic paint
Magnetic photocatalyst
Zinc ferrite

ABSTRACT

In the present study, we report the synthesis and application of $ZnFe_2O_4/SiO_2$-TiO_2 nanocomposites with non-stoichiometric content of Fe to Zn used for the first time for the preparation of new generation trifunctional paints with self-cleaning, biocidal and magnetic properties. Currently, there are no compositions on the market for obtaining protective coatings in the form of paint, which simultaneously exhibit biocidal, magnetic and self-cleaning - photocatalytic properties. The effect of Zn:Fe content on the antimicrobial, magnetic and self-cleaning properties of obtained modified paints was investigated. Furthermore, the non-stoichiometric zinc ferrite in combination with TiO_2 allowed to create of a surface that inhibits microorganisms' growth. Self-cleaning properties were studied in the reaction of dye - neutral red degradation. The commercial white paint was not photocatalytic active. Paint modification with nanocomposites based on $ZnO/ZnFe_2O_4$ and TiO_2 resulted in the effective degradation of natural red dye. The highest dye removal efficiency was observed for the sample containing $ZnFe_2O_4/SiO_2$-TiO_2 particles with a non-stoichiometric 1:2 (Fe: Zn) molar ratio. Trifunctional paints with photocatalytic, magnetic and biocidal properties are a novelty in building products. The composition can be applied to protective and decorative layers, giving magnetic, biocidal and self-cleaning properties.

1. Introduction

In the last few decades, indoor air quality IAQ (Indoor Air Quality) has become one of the most important factors determining health, comfort and well-being because people spend most of their daily time indoors, where they are routinely exposed to indoor pollutants.

According to World Health Organization (WHO), around a third of the global population is exposed to dangerous levels of household air pollution while using inefficient stoves fuelled by kerosene, biomass and coal [1]. The indoor air quality is influenced by outdoor pollutants associated with vehicular traffic and industrial activities, which can enter by infiltrations and ventilation systems. Moreover, indoor pollutants originate inside the building from cleaning products, furnishings, central heating, electronic equipment, and kinds of activities undertaken by users, such as cooking, frying, using candles and incense, smoking tobacco, and burnings fuels [2,3]. Making buildings more energy efficient will contribute to the sealing of windows and doors and result in the accumulation of indoor pollutants and air stagnation; as a consequence increase in IAQ is observed.

The most abundant groups of indoor air pollutants are chemical compounds (e.g., nitrogen oxides, carbon oxides, volatile organic compounds, formaldehyde, phthalates, nitrosamines, polycyclic aromatic hydrocarbons, particulate matter) or biological agents, including viruses, bacteria, fungi in particular filamentous fungi (mould), parasites or parts of a plant, which can induce adverse human health impacts [4,5]. Some toxigenic moulds growing in damp indoor spaces also produced mycotoxins – secondary metabolites with diverse structures. All of them pose a health hazard to humans and animals [6]. The chemical and biological contaminants contribute to sick building syndrome (SBS), defined as a condition in which occupants in a building suffer from symptoms such as irritation of the eyes, nose, and throat, headache, dizziness, and fatigue [7]. Prolonged exposure to indoor air pollutants can trigger symptoms of asthma or allergies. Moreover, air pollution is the cause and aggravating factor of many respiratory diseases like chronic obstructive pulmonary disease (COPD), lung, laryngeal or nasopharyngeal cancer and skin diseases, e.g. mycoses. A higher

* Corresponding author. Narutowicza 11/12, 80-233, Gdańsk, Poland.
E-mail address: annjurek@pg.edu.pl (A. Zielińska-Jurek).

https://doi.org/10.1016/j.ceramint.2023.10.166
Received 20 June 2023; Received in revised form 12 October 2023; Accepted 16 October 2023
Available online 18 October 2023

proportion of individuals presenting mentioned symptoms are infants, the elderly, a person with chronic disease, and most urban dwellers of any age [8]. Therefore, the removal of indoor air pollutants is crucial to prevent health issues.

Furthermore, microorganisms growing on building materials cause physical and chemical damage referred to as biodetortiation. The highly susceptible to microbial growth are organic building materials containing cellulose, e.g., paints, varnish coatings, and plasters [9,10]. The best biocides are chemical compounds with a broad spectrum of activity on various species of microorganisms, such as bacteria, fungi or other microorganisms [11]. The nanotechnology, and more specifically, nanocomposite formulations with strictly defined sizes and shapes of nanoparticles, resulted in the preparation of nanomaterials with antimicrobial properties [12–15]. The first reports on nanoparticles application in paint to prevent the settlement and growth of different biofouling organisms with a reduced negative effect on the environment appeared in 2006 when Nyden et al. received a patent on a method for application of Cu, ZnO, TiO_2, CuO nanoparticles as biocides in paints [16]. The paint consists of a composition based on imidazoles bound to metallic nanoparticles with a developed surface area for the adsorption of pathogenic microorganisms.

Heterogeneous photocatalysis is one of the most promising methods of air pollutants degradation and surface disinfection [17,18]. At present, titanium (IV) oxide is the most extensively studied and widely applied material with photocatalytic properties because it is relatively inexpensive and has a high oxidation potential [14]. It is also worth mentioning the excellent photostability, photoactivity and superhydrophilicity compared to other materials [19]. Photocatalytic TiO_2--based products, such as plasters, coatings, paints, concretes, floors, and tiles, have wide applications in many construction market segments [14]. The materials mentioned above possess the properties of air pollution removal and self-cleaning [15,17,20–22].

However, TiO_2 exhibits one fundamental disadvantage - it can be activated only by UV light due to its absorption edge below 400 nm. Therefore, over the past few decades, many modifications like dye sensitisation and doping with metal and metal oxide or non-metal anions have been proposed to improve TiO_2 activity and sensitivity under visible light [23–25]. Overcoming the limitations of titanium (IV) oxide has led to broadening the scope of offered products. Jiang et al. [25] obtained nano-TiO_2 coated glasses modified by doping with N, F, and Fe ions. The slides prepared were used for the degradation of air pollutants in visible light. The TiO_2-modified glass exhibited superhydrophilic properties for self-cleaning applications. New generation of photocatalytic paints for indoor applications could help improve air quality and allow the creation of surfaces that kill or inhibit the growth of microorganisms. Analysing the construction market, one can notice a gap in which hybrid paints are missing, with the property of simultaneously removing indoor air pollutants, magnetic and biocidal properties.

In this regard, the aim of the present study was the synthesis and application of ZnO/$ZnFe_2O_4$/SiO_2-TiO_2 nanocomposites used for the first time for the preparation of trifunctional paints with self-cleaning, biocidal and magnetic properties. The photoactivity and biocidal properties of two new TiO_2-based paints and one commercial under natural indoor light were investigated. The method of preparation of magnetic photocatalytic composites with a controlled core-interlayer-coating structure allows the functionality of a magnetic core with a silica interlayer and a TiO_2 photocatalytic layer. The ferrite particle may interact with silica, while TiO_2 nanoparticles may interact with silica particles embedded in the ferrite core [26]. The application of zinc compounds, which are safe for humans and animals and widely used in pharmacy [27] and cosmetology [28], provided the composite with biocidal (ZnO) and magnetic ($ZnFe_2O_4$) properties. Furthermore, $ZnFe_2O_4$ as a zinc spinel ferrite at the nanoscale reveals superparamagnetic properties, providing the coating magnetic properties [29]. Introducing a silica layer in the ZnO/$ZnFe_2O_4$/SiO_2-TiO_2 composite structure enhanced paint dispersion and increased the adhesion of pollutant particles on the surface of the self-cleaning layer, enabling photodegradation of the organic pollutants and microorganisms. The effect of Zn: Fe content on the antimicrobial, magnetic and self-cleaning properties of obtained modified paints was investigated.

2. Materials and methods

2.1. Materials

Commercial TiO_2 P25 (mixture of the crystalline phases: anatase and rutile, $S_{BET} = 50\ m^2g^{-1}$, particle size: 20 nm) was provided by Evonik (Germany). Zinc (II) chloride, iron (II) sulfate heptahydrate, and sodium hydroxide were purchased from Aldrich.

2.2. Synthesis of $ZnFe_2O_4$

Firstly, to obtain zinc ferrite particles, $FeSO_4 \bullet 7H_2O$ and $ZnCl_2$ were dissolved in non-stoichiometric 1:2 (Fe: Zn) and 1:1.5 (Fe: Zn) molar ratio in deionised water under stirring (500 rpm) for 30 min. Afterwards, the metals were precipitated from the homogenous solution by adding 5 M NaOH at room temperature to a pH of 10. The reaction mixture was hydrothermally treated in an autoclave at 200 °C for 5 h. Subsequently, the solid product of the reaction was magnetically separated and purified with deionised water several times. The final product was dried to dry mass. The proposed method of synthesis allows to obtain hybrid nanocomposites of nanometric sizes.

2.3. Synthesis of $ZnFe_2O_4$/SiO_2-TiO_2 nanocomposite

In the next synthesis step, the nanoparticles were re-dispersed in a mixture of 0.1 M Triton X-100, cyclohexane, isopropanol and water. Then, tetraethyl orthosilicate (TEOS) was added to the suspension to obtain a silica layer and ammonia water as a precipitating agent. The molar ratios of TEOS to ZnFe2O4 and NH4OH to TEOS were equal to 8:1 and 16:1, respectively. The pH of the mixture was reduced below 5, and TiO_2 P25 was added. The content of zinc spinel ferrite to TiO_2/SiO_2 was 20 % by weight. Then, the obtained suspension was magnetically separated, washed with acetone and deionised water, and dried at 70 °C to dry mass. The obtained ZnO/$ZnFe_2O_4$/SiO_2-TiO_2 composite was calcined at 400 °C for 2 h.

2.4. Preparation of bio-photo-magnetic paint

Bio-Photo-Magnetic paint was prepared according to the scheme presented in Fig. 1. The commercial white paint and powder composite of ZnO/$ZnFe_2O_4$/SiO_2-TiO_2 were mixed with a mechanical stirrer in the proportion of 3 g of composite for 50 dm^3 of paint.

2.5. Characterisation of materials

Firstly, the phase structure of the ZnO/$ZnFe_2O_4$/SiO_2-TiO_2 composites was analysed with the powder X-ray diffraction (XRD) method using Rigaku MiniFlex 600 X-ray diffractometer (Rigaku Corporation, Tokyo, Japan). The patterns were obtained in step-scanning mode ($\Delta 2\theta = 0.01°$) in the range from 10° to 80° 2θ. Nitrogen adsorption-desorption isotherms were analysed using the Micromeritics Gemini V instrument. Diffuse reflectance spectra (DR) in the 300–800 nm range were measured using ThemoScientific Evolution 220 Spectrophotometer (Waltham, MA, USA) equipped with PIN-757 integrating sphere. The composite surface morphology was examined by scanning electron microscopy (SEM) using SEM Microscope FEI Quanta FEG 250. The magnetic properties of coated ferrite nanocomposites were investigated using the Physical Properties Measurements System (Quantum Design, San Diego, CA, USA) at 293 K and in the range of 0–3 T.

The surface area was determined using the BET isotherm method (Brunauer, Emmett and Teller) using the Micromeritics Gemini V

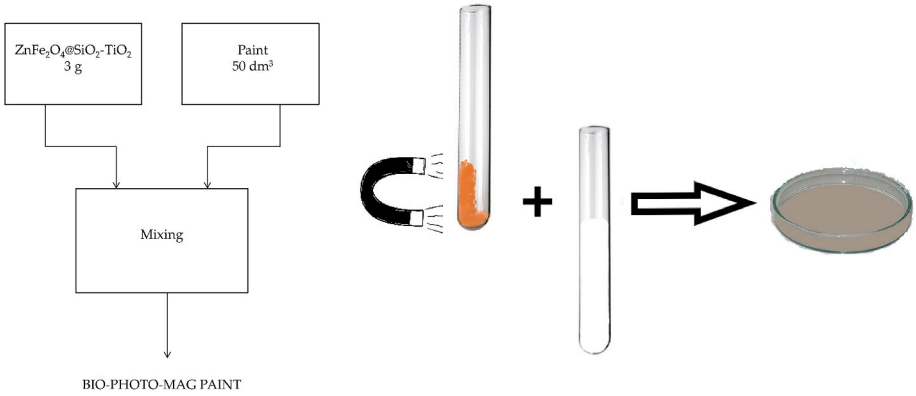

Fig. 1. Schematic illustration of the preparation method of bio-photo-magnetic paint.

apparatus. The analysed samples, weighing 0.3 g, were degassed for 2 h at 200 °C in the Micromeritics FlowPrep 060. Then, the amount of adsorbed nitrogen on the surface of the photocatalysts was determined. Adsorption occurred at a temperature of 77K, the boiling point of liquid nitrogen. The carrier gas in the system was helium. Changes in the thermal conductivity of the gas mixture reflect changes in the adsorption and desorption processes. From the determined adsorption isotherm using the Brunauer, Emmett and Teller equation, the specific surface area of the tested nanocomposites was calculated according to the equation:

$$\frac{x}{a(1-x)} = \frac{1}{a_m K} + \frac{K-1}{a_m K} x$$

where: x - relative pressure in the range of 0.04–0.05; am - capacity of the absorption monolayer, K - adsorption equilibrium constant.

2.6. Self-cleaning properties of trifunctional paints

Transparent plastic foils, in the shape of squares with a side of 5 cm, were covered with zinc ferrite (sample S1 and S2), modified paints containing nanocomposite particles (samples S3 and S4), and a sample of white paint (sample S0, which served as a reference sample). The samples prepared in this way were placed in the dye solution for 45 min, dried at 40 °C and irradiated. Photocatalytic degradation of natural red dye was performed using a 300W Xenon lamp emitting UV–vis light. The degradation of the dye was calculated from the reduction in absorption intensity of natural red dye in the concentration c = 0.02 $\frac{\text{mol}}{\text{dm}^3}$ at a fixed wavelength k_{max} = 550 nm. The degradation efficiency was then calculated as given in PD = $\frac{C_0 - C}{C_0} * 100\%$, where C_0 is the initial concentration of the natural red and C is the concentration after irradiation at given time intervals. The total irradiation time was 120 min.

2.7. Antimicrobial properties of trifunctional paints

The antimicrobial properties of paints were determined using Gram-negative bacteria *Escherichia coli* K12 (ATCC 29425) and Gram-positive bacteria *Staphyloccocus epidermidis* (ATCC 49461). The test microorganisms were cultivated in two types of liquid media – nutrient broth (NB) for *E. coli* and Brain-Heart Infusion (BHI) for *Staphylococcus epidermidis* and incubated for 24 h at 37 °C Then test culture was diluted using 0.85 % sterile sodium saline buffer to the final concentration 0.5 in McFarland standard to a final concentration approx. 1.5×10^6 CFU/ml The experiments were carried out according to ASTM E2149-01: Standard test method for determining the antimicrobial activity of antimicrobial agents under dynamic contact conditions with some modifications [30]. For the antibacterial performance examination, the sheets of paper covered by paints or sheet paper (as negative control) were cut into small pieces and 1.0 ± 0.1 g were transferred into a sterile 250 mL screw-cap Erlenmeyer flask for each treated (paper covered by paints) and untreated specimen (uncovered by paints). Then, 50 ± 0.5 mL of working dilution of bacterial inoculum prepared flask. The flasks were placed on the wrist-action shaker and were shaken for 1.0 h ± 5 min. The experiments were carried out under visible (one bulb 300 W, OSRAM Ultra Vitalux, Poland) irradiation placed about 15 cm from the flask and under dark conditions. The radiant flux was monitored with a radiation intensity meter LB901 (Lab-EL, Poland) equipped with CM3 and PD204AB Cos sensors. Immediately serial dilute and plate each sample out in triplicate, as was done for the "0" contact time subgroup. The samples were collected after 0.5 and 1.5 h. Serial tenfold dilutions using 0.85 % sodium saline solution were made, and 0.25 ml were plated on appropriate solid media: Standard Plate Count Agar (PCA) for *E. coli* and Brain-Heart Infusion Agar (BHI) for *S. epidermidis*. The inculcated plates were incubated at a temperature of 37 °C for 24 h. Then the visible colonies were counted and shown as log CFU/mL. The antimicrobial activity was expressed as bacterial survival rate after contact with the painted paper and control sample.

The trifunctional paints were coated on paper using a K-paint coater at a speed of 1 cm/min and 2 μm. The samples were dried for at least 48 h before antimicrobial analyses. The coated papers were cut to 1.5 cm × 1.5 cm squares. The agar plate method was used for the evaluation of antimicrobial effect of the coatings. Gram-positive *Staphylococcus aureus* (ATCC 6538) and gram-negative *Escherichia coli* (ATCC 10536) were used to test the antibacterial activity of modified paints. For disc diffusion sensitivity tests, the semi-liquid medium was inoculated with 10^5 cells/ml of an overnight culture of microbial cells, poured into Petri plates and left for solidification. The paint samples were placed on the agar medium surface. Plates were incubated for 24 h at 37 °C. The zones of inhibition were measured.

3. Results

3.1. Characterisation of $ZnO/ZnFe_2O_4/SiO_2$-TiO_2 composites

The magnetic properties depend on the preparation method, grain size, cation distribution and calcination temperature. Bulk $ZnFe_2O_4$ is a normal spinel, where Fe^{3+} cations antiferromagnetically coupled occupy octahedral (B) sites, and Zn^{2+} cations (non-magnetic) are preferentially located at the tetrahedral A positions [31]. However, at the nanoscale, zinc ferrite nanoparticles exhibit cationic inversion between octahedral and tetrahedral sites and the occurrence of mixed states (i.e., Fe^{3+} cations in both B and A sites) is noticed [29]. The *M–H* curves of $ZnFe_2O_4$ NPs and composites are presented in Fig. 2. The hysteresis loop can be used to read the magnetic parameters such as saturation magnetisation (Ms), coercivity (Hc), and remanent magnetisation (Mr). The values are presented in Table 1. At RT, these values for S1 were 44 emu/g, 0.02 kOe, and 7.6 emu/g, respectively. The saturation

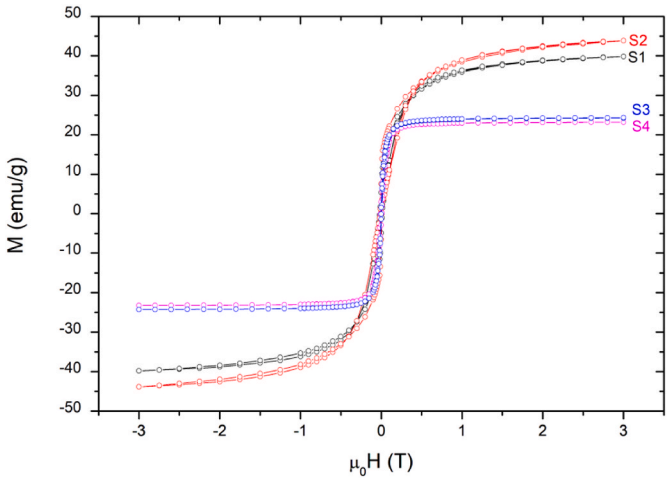

Fig. 2. Magnetic hysteresis loops of magnetic core $ZnFe_2O_4$ and nanocomposites of ZnO/ZnFe $_2O_4$/SiO_2-TiO_2.

magnetisation for sample S2 was slightly lower and equalled 40 emu·g^{-1}. The decrease in the magnetisation of S2 could be related to different cation distribution or the occurrence of some amount of the sample non-ferrimagnetic (ZnO). At 300 K, the coercivity was close to zero, which shows that samples S1 and S2 are superparamagnetic. This is well expected, as for a superparamagnetic system, the coercivity is zero [32, 33]. In addition, besides the cation distribution, the magnetic properties of nanostructured ferrites depend on microstructures such as crystallinity and crystallite size. For magnetic spinel ferrites, the critical size is around 30–40 nm [34,35]. When the particle size is reduced below the critical size, it becomes superparamagnetic, with zero coercivity. Due to a crystallite size of about 8–9 nm, the obtained ferrimagnetic zinc ferrite particles can behave superparamagnetically at RT. After coating with TiO_2 and silica layer, the magnetisation of the nanocomposite decreased from 44 to 40 emu·g^{-1} to 23–24 emu·g^{-1}. The decrease in magnetisation should be related to the mass contribution of the SiO_2 and TiO_2 coating. It was expected since $ZnFe_2O_4$ is a small fraction of the final material (calculated to 5 wt %). As revealed by the XRD analysis, TiO_2 and SiO_2 are predominant in both S3 and S4 samples, and therefore the magnetisation decrease should be proportional to their content.

The physicochemical characteristics of the composites, e.g., crystallite sizes, indirect band gap values, BET surface areas, are presented in Table 1. The BET surface area of both zinc ferrite samples (S1 and S2) was about 20 m^2 g^{-1}. The specific surface area of nanocomposites coated with SiO_2-TiO_2 was about 52 m^2 g^{-1}, similar to that of TiO_2 P25 (50 m^2 g^{-1}).

The XRD patterns of zinc ferrite particles (samples S1 and S2) and ZnO/$ZnFe_2O_4$/SiO_2-TiO_2 composites (samples S3 and S4) are presented in Fig. 3. The formation of $ZnFe_2O_4$ was confirmed by the presence of signals at 2θ 29.8°, 35.2°, 42.8°, 53.1°, 56.5° and 62.1°, according to JCPDS No. 82–1042. Moreover, due to the non-stoichiometric content of Fe:Zn during the synthesis, the characteristic diffraction peaks for produced in situ hexagonal wurtzite structure of ZnO at 2θ 32.6°, 36.0° and 62.8° can be noticed (JCPDS card no. 36–1541). The diffraction peaks at 2θ 25.3°, 36.9°, 48.0° and 53.9° corresponds to the of anatase TiO_2 (JCPDS No. 89–4203). Deposition of both SiO_2 and TiO_2 layers resulted in visible weakening of $ZnFe_2O_4$ signals at 2θ 35.2° for samples S3-S4. Crystallite sizes of zinc ferrite and TiO_2 (anatase) particles were determined using the Scherrer equation and equalled 8–8.5 nm and 20 nm, respectively.

The optical absorption properties of the nanomaterials are presented in Fig. 4. The analysed samples absorb UV light due to the sp-d interaction between valence band electrons of O and d electrons of Ti or Zn/Fe atoms in TiO_2 and $ZnFe_2O_4$ structures, respectively. The higher absorption properties of S2 than S1 resulted from the presence of a higher amount of ZnO in the heterostructure. Obtained spectra were transformed into the Kubelka-Munk function, and the Tauc transformation was used to determine the band gap values. The band gap for the two samples S1 and S2 was in the range of 1.75–1.85 eV. Different synthesis methods and different parameters of zinc ferrite synthesis result in the various energy band values of zinc ferrite nanoparticles. Lemine al [36]. reported the band gap of $ZnFe_2O_4$ of about 2.23 eV. Gao et al. [37] reported a band gap energy of 1.9 eV for nanocrystalline $ZnFe_2O_4$ synthesised with a polymer complex.

The morphology of the samples was examined by scanning electron microscopy and transmission microscopy analyses, and the results are presented in Fig. 5. The zinc ferrite particles grow in situ on the surface of ZnO, forming a special 3D flower-like structure [38,39]. For magnetic photocatalysts of ZnO/$ZnFe_2O_4$/SiO_2-TiO_2 the spherical morphology of the particles can be noticed due to the coating of zinc ferrite with a protective SiO_2 and TiO_2 layer. Based on TEM analysis, the particle size for sample S4 was about 50 nm. The different values of particle size of TEM and crystal size of XRD analysis result from the structural properties and lattice strain as a result of clustering of the nanoparticles. The average particle size of the samples is larger than the crystallite size calculated based on the Scherrer equation. However, the obtained results suggest that the zinc ferrite core (~8 nm) is coated with a SiO_2-TiO_2

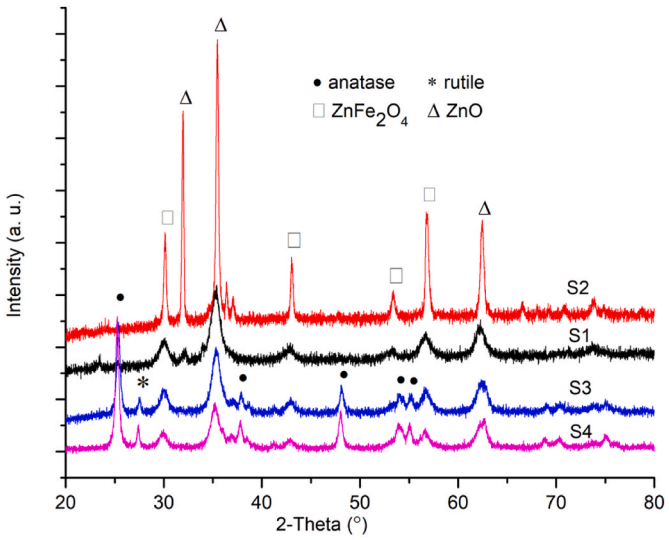

Fig. 3. XRD patterns of samples S1-S4.

Table 1
The physicochemical characteristics of $ZnFe_2O_4$ and $ZnFe_2O_4$/SiO_2-TiO_2.

Sample	Molar ratio	Ms (emu·g^{-1})	Hc (T)	Mr (emu·g^{-1})	BET (m^2·g^{-1})	Pore volume (cm^3/g)	Eg	Crystallite Size (nm)		
								Anatase	Rutile	Zinc Ferrite
S1 $ZnFe_2O_4$	Fe:Zn 1:1.5	44	0.002	7.6	20	0.0021	1.75	–	–	8.0
S2 $ZnFe_2O_4$	Fe:Zn 1:2	40	0.018	5.4	21.5	0.0103	1.85	–	–	8.5
S3 $ZnFe_2O_4$/SiO_2-TiO_2	Fe:Zn 1:1.5	24	0.002	1.43	49	0.0017	1.9	20	32.5	8.0
S4 $ZnFe_2O_4$/SiO_2-TiO_2	Fe:Zn 1:2	23	0.010	2.9	52	0.0011	2.1	20	31.0	8.5

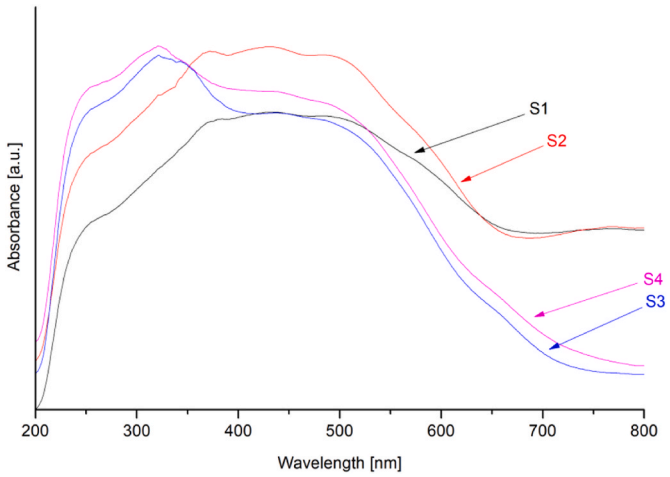

Fig. 4. Diffuse reflectance spectra of sample S1-S4.

shell (~30 nm).

Furthermore, the SEM images of white commercial paint, $ZnFe_2O_4$ modified paints and $ZnO/ZnFe_2O_4/SiO_2$-TiO_2 modified paints are presented in Fig. 6. The powder modifier is located on the upper surface, which allows for full activation of the composite components responsible for the trifunctional properties of the paint.

3.2. Photocatalytic properties of trifunctional paints

The images of paint coatings are presented in Fig. 7. The paint samples, after modification with $ZnFe_2O_4$ and $ZnO/ZnFe_2O_4/SiO_2$-TiO_2 were different shades of beige (S1-S4). The S0 sample is a reference sample coated with commercial white paint.

The self-cleaning properties of $ZnO/ZnFe_2O_4/SiO_2$-TiO_2 – modified paint (sample S4) are presented in Fig. 8. After the dyeing process, the sample was uniformly red colour (Fig. 8a). Furthermore, the photodegradation process led to efficient dye degradation and the sample returned to its original colour (Fig. 8b). The photocatalytic activity of paint layers (self-cleaning properties), including the un-modified commercial paint (sample S0), are presented in Fig. 9. For the reference sample S0, the photodegradation was not observed, which is a natural phenomenon for unmodified paint. For samples S1 and S2 of paint modified with zinc ferrite nanoparticles with a non-stoichiometric Fe:Zn content, the dye degradation efficiency was about 47.5% and 56.6%, respectively. Paint modification with nanocomposites based on $ZnFe_2O_4$ and TiO_2 resulted in the effective degradation of natural red dye. The highest photodegradation efficiency of about 93% was observed for sample S4 containing $ZnO/ZnFe_2O_4/SiO_2$-TiO_2 composite with Fe:Zn ratio of 1:2. For sample S3 the observed self-cleaning properties were slightly lower, and the efficiency of decolourisation of the surface reached about 86.2%. The difference results from the increased content of ZnO in $ZnFe_2O_4/SiO_2$-TiO_2 (sample S4, Fe:Zn equalled to 1:2) composite structure, which is a consequence of the photocatalyst synthesis method.

3.3. Antimicrobial properties of trifunctional paints

Photocatalytic inactivation of *Escherichia coli* and *Staphylococcus epidermidis* was analysed on paper sheets covered by commercial and modified with $ZnO/ZnFe_2O_4/SiO_2$-TiO_2 composites paints according to ASTM E2149-01 recommended for testing antimicrobial additives. All tests were conducted in dark conditions or under visible light. Fig. 10 a-b shows the photocatalytic inactivation of *E. coli* and S. *epidermidis* bacteria. The inactivation of bacteria on control paper sheets was significantly lower (almost 100% of survival bacteria), independently from lighting conditions.

These study showed that for activation of $ZnO/ZnFe_2O_4/SiO_2$-TiO_2 also, visible light (indoor light) can be used. The paints containing $ZnO/ZnFe_2O_4/SiO_2$-TiO_2 particles showed good antimicrobial activity against both tested bacteria under visible light conditions. After 1h of

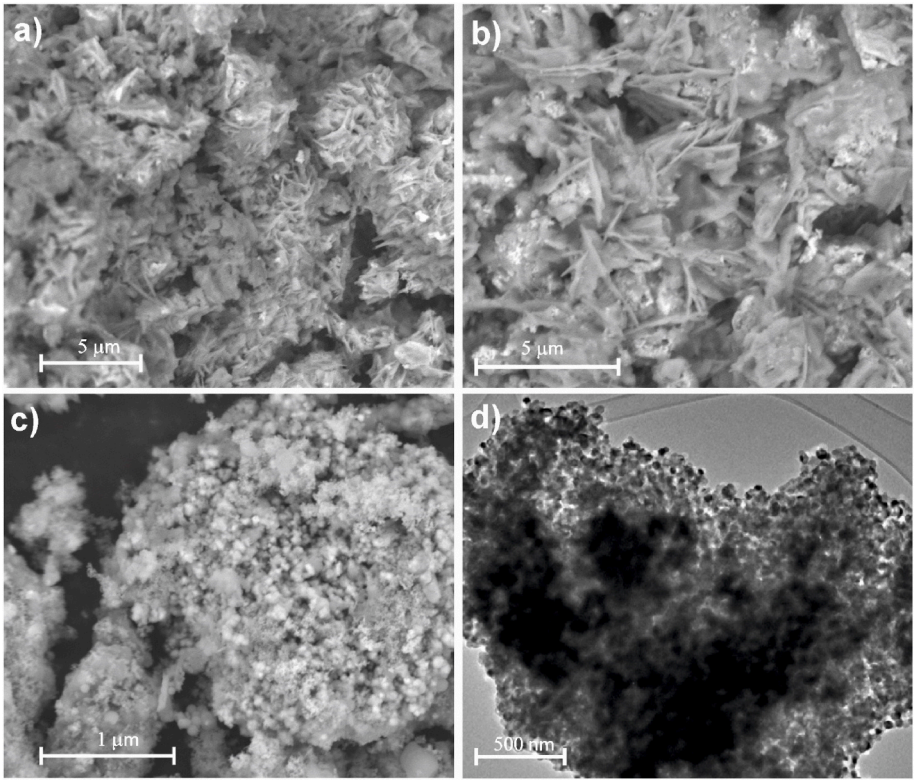

Fig. 5. Microscopy SEM images of samples S1 (a), S2 (b), S4 (c), and TEM image of $ZnO/ZnFe_2O_4/SiO_2$-TiO_2 composite (sample S4).

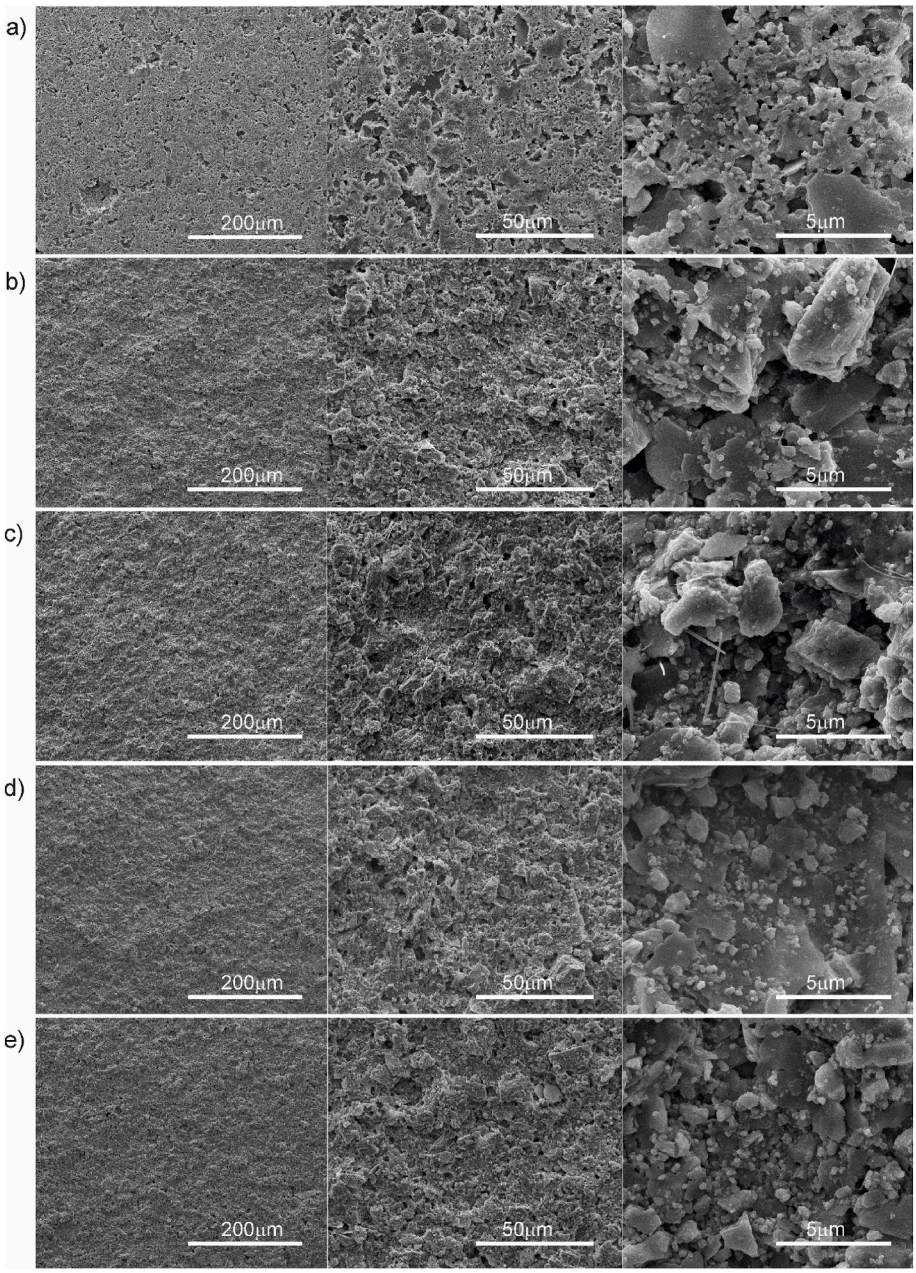

Fig. 6. The morphology (SEM images) of white commercial paint S0 without additives (a), modified paints with $ZnFe_2O_4$ (S1-S2) (b,c) and $ZnO/ZnFe_2O_4/SiO_2$-TiO_2 (S3-S4) samples (d,e).

exposition, almost half of the bacteria were inactivated (Fig. 10 a-b). The experiment indicated a synergy between the molar ratio of Fe: Zn and antibacterial properties. The higher concentration of zinc effectively inhibited the growth of bacteria Gram negative E. coli and Gram positive S.epidermidis due to in situ formation of $ZnO/ZnFe_2O_4$ particles. Gram negative bacteria were more sensitive than Gram positive. *E. coli* showed a higher $\log_{10}$ reduction in colony-forming units (CFU/mL) than the *S. epidermidis* after 1 h. The efficiency of both bacteria inactivation for $ZnFe_2O_4/SiO_2$-TiO_2 (Fe:Zn 1:2) paint under visible light activation was comparable to commercial paint. As presented in Fig. 11, based on XRD analysis, the presence of Zn was confirmed in the commercial paint structure.

However, due to the paint composition being only known to the producer, it was impossible to specify inhibition or stimulation agents. The maximum reduction of *E. coli* bacteria under vis irradiation was: 3.26 log for $ZnFe_2O_4/SiO_2$-TiO_2 (Fe:Zn 1:2) paint, 3.2 log for commercial paint and 1.16 for $ZnFe_2O_4/SiO_2$-TiO_2 (Fe:Zn 1:1.5). In the same conditions for *S. epiderimidis* the reduction rate was 2.62, 2.82 and 0.92 respectively. As reported by Zuccheri et al. the photocatalytic agent in commercial paints is used at a very high concentration in the range of 15 vol % – 80 vol % [40]. Moreover a significant bacterial inactivation of about 90 % (investigated only against *E. coli*) was reached only after 48 h of irradiation with UV lamp. It is well known that the antibacterial activity of photocatalytic products such as paints is related to efficiency in generating ROS under light irradiation [40–42]. Both tested in this study bacteria are facultative anaerobic organism that causes higher sensitivity to oxygen exposure and have weaker mechanisms of ROS neutralisation (in contrast to aerobic organisms) [43]. Another possible explanation was demonstrated by Hochmannova and Vytrasova [44]. The authors concluded that zinc-containing formulations (paints) exhibit a few times higher antimicrobial efficiencies than nano TiO_2 paints. In an aqueous solution, Zn^{2+} ions can damage the cytoplasmic

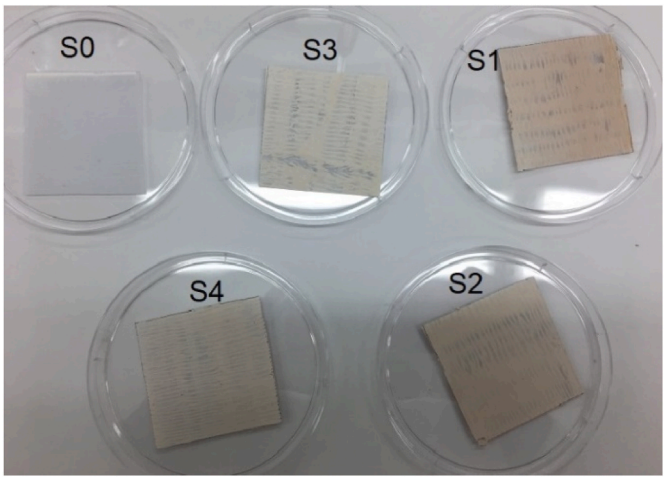

Fig. 7. Paint samples modified with $ZnFe_2O_4$ (S1-S2), $ZnFe_2O_4/SiO_2$-TiO_2 (S3-S4) and S0-white paint before the dying process.

membrane and act as an inhibitor of the glycolytic enzyme through the thiol group oxidation [45]. It is noteworthy that $ZnO/ZnFe_2O_4/SiO_2$--TiO_2 modified paints also revealed excellent antimicrobial properties in darkness (Fig. 10).

Furthermore, it is also possible that electrostatic interactions of nanoparticles play a crucial role in this process. Metal nanoparticles of Cu, Ag and Zn are positively charged and can bind to the negatively charged bacterial cell via electrostatic repulsion. It can cause direct disruption of electron transport chain or even mechanical damage of cell walls. Both these abnormalities can lead to bacteria death [46]. As summarised Kirthika et al., metal and metal oxide nanoparticles (e.g. ZnO, MgO CuO, TiO_2 etc.) are classified as active antimicrobial agents (AAA), which means that they eradicate microbes completely by varied mechanisms of action. In contrast, passive antimicrobial agents (PAA) only prevent the growth of microbes [47]. Many of the listed above NPs exhibit a biocidal activity against Gram-positive and Gram-negative bacteria or microscopic fungi isolated from varied environments (human body, water, air etc.), which was described in a wide range of review papers [17,46–50]. Nevertheless, the mechanism of their antimicrobial action is not fully known. On the one hand, it is due a variation and evolution in microorganisms, but on the other, it is caused by rapid progress in the method of synthesis of nanoparticles characterised by their different size, shapes, composition or physical properties. Additionally, in the case of self-cleaning and self-disinfecting building materials such as paints or coatings, the synergistic effect of NPs in combination with polymers and chemicals used as a component of the final product determines the antibacterial efficacy of a surface [51].

Finally, the inhibition zones against microorganisms for zinc ferrite modified paints with a non-stoichiometric Fe:Zn content were analysed and compaed with the inhibition zones of stoichiometric zinc ferrite ($ZnFe_2O_4$) modified paint and white paint without additives as reference. In Table 2, the diameters of zones of inhibition for modified paints are presented. The labels in the first column are the same as in Figs. 7–11, and are related to zinc ferrite modified paints and $ZnO/ZnFe_2O_4/SiO_2$-TiO_2 modified paints. The best antimicrobial activity was observed for samples S1 and S3 prepared using non-stoichiometric $ZnFe_2O_4$.

The zones of inhibition against *St. aureus and E. coli* were observed for samples of paints S1, S3 and S5. Our results are in good agreement with others. Mandal et al. reported that zinc ferrite nanoparticles revealed similar biocidal properties to known antibiotics on many bacterial colonies [52]. García-Cruz et al. demonstrated the activity of zinc ferrite nanoparticles against phytopathogenic bacteria [53]. The highest antibacterial activity was observed for S3 and S1. However, broad inhibition zones of the growth of both bacterial colonies for S1 and S3 samples are clearly visible. The observed inhibition zones are twice as

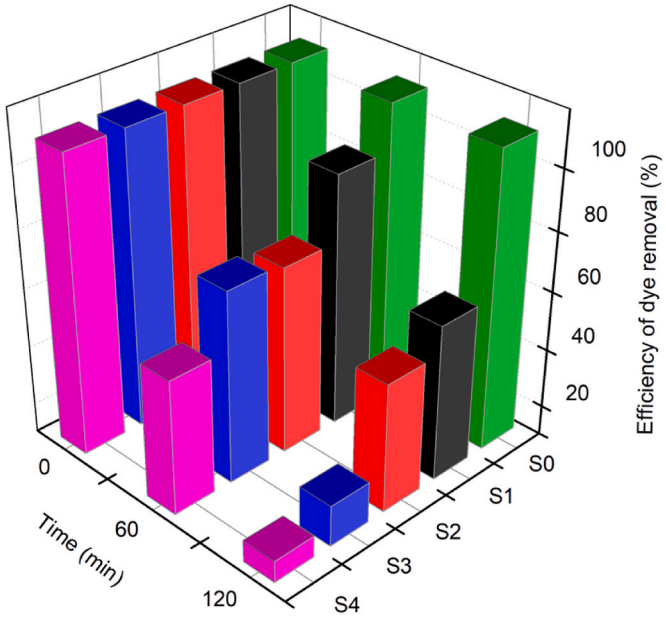

Fig. 9. The results of photocatalytic degradation of dyes for paint samples S1-S4 and control sample S0 (white paint without modification).

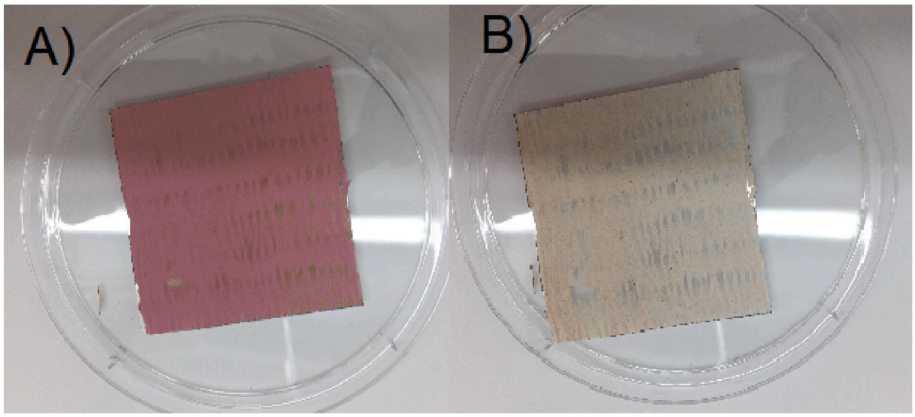

Fig. 8. The images of sample S4 before the dye (natural red) photodegradation process (a) and after the photodegradation process (b). (For interpretation of the references to colour in this figure legend, the reader is referred to the Web version of this article.)

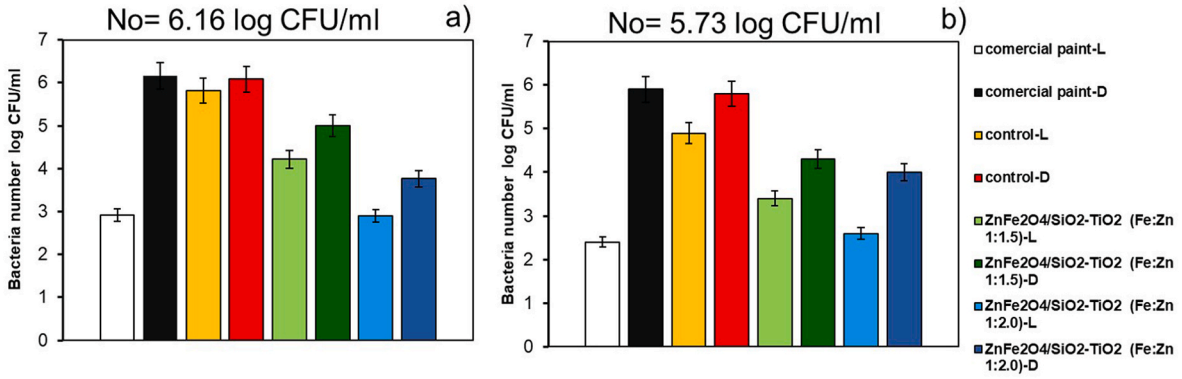

Fig. 10. Effect of photocatalytic paints on inactivation of bacteria a) *E. coli* b) *S. epidermidis* after 1.0 h exposure to L – light or D – dark conditions; control – uncovered paper (negative control), No – initial number of bacteria (time 0 h).

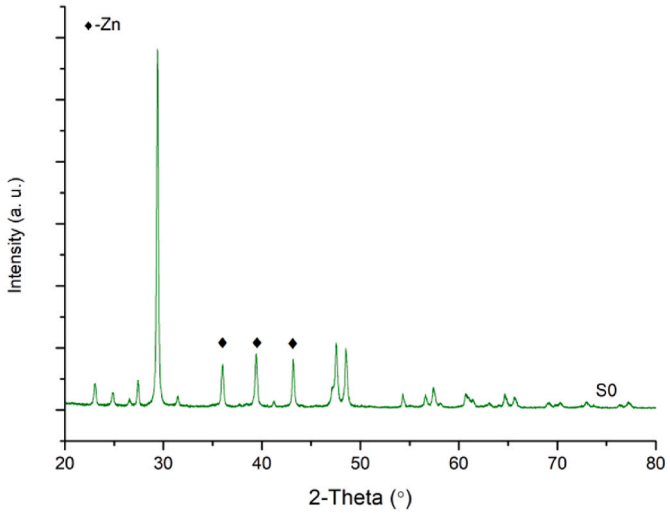

Fig. 11. XRD pattern of commercial white paint.

Table 2
The inhibition zones against microorganisms for trifunctional paints and commercial paint.

Trifunctional paint		Zone of inhibition (mm)	
Sample label	Description	*Staphylococcus aureus* ATCC 6538	*Escherichia coli* ATCC 10536
S0	white paint without additives	0	0
S1	non-stoichiometric $ZnFe_2O_4$ (Fe:Zn 1:1.5) modified paint	21.3	32.9
S3	non-stoichiometric $ZnFe_2O_4$/SiO_2-TiO_2 (Fe:Zn 1:1.5) modified paint	19.6	33.8
S5	stoichiometric $ZnFe_2O_4$ modified paint	11.2	18.9

wide compared to stoichiometric $ZnFe_2O_4$. The in situ generation of zinc oxide into the structure of zinc ferrite markedly improved the original biocidal properties of pure stoichiometric zinc ferrite.

4. Conclusions and discussion

In the present study, a composition containing an active agent - a composite based on TiO_2, ZnO and $ZnFe_2O_4$ with a non-stoichiometric Fe:Zn content and the method of producing this trifunctional paint was for the first time reported.

Nanocomposites with biocidal, magnetic and self-cleaning properties were characterised to confirm the effectiveness of the product in the form of trifunctional paint concerning magnetic properties (analysis of magnetisation saturation), biocidal properties (analyses concerning Gram-positive *Staphylococcus epidermidis* and Gram-negative *Escherichia coli*, and self-cleaning properties in the neutral red dye degradation reaction.

The obtained ferrimagnetic zinc ferrite particles revealed superparamagnetic properties at room temperature. The formation of $ZnFe_2O_4$ was confirmed by XRD analysis. Moreover, due to the non-stoichiometric content of Fe:Zn during the synthesis, the characteristic diffraction peaks for hexagonal wurtzite structure of ZnO were noticed. The composite with a surface area of about 50 $m^2 \cdot g^{-1}$, particles size 50 nm and UV–Vis light absorption properties possessed saturation magnetisation of 24 $emu \cdot g^{-1}$, magnetic coercivity of 0.010 T and remanent magnetisation of 2.9 $emu \cdot g^{-1}$. Furthermore, the self-cleaning properties of $ZnO/ZnFe_2O_4/SiO_2$-TiO_2 were confirmed. Paint modification with nanocomposites based on $ZnFe_2O_4$ and TiO_2 resulted in the effective degradation of natural red dye. The paints containing $ZnO/ZnFe_2O_4/SiO_2$-TiO_2 particles showed high antimicrobial activity under visible light conditions.

Currently, there are no compositions on the market for obtaining protective coatings in the form of paint, which simultaneously exhibits biocidal, magnetic and self-cleaning - photocatalytic properties. The synthesised and characterised trifunctional compositions with photocatalytic, magnetic and biocidal properties are a novelty in building industry products. The composite can be added at different stages of paint formulation, confirming the high efficiency in the elimination of pathogenic microorganisms, self-cleaning properties and the magnetic effect that can be applied to different surfaces. The proposed product – trifunctional paint, enriches the market offer in the broader building products industry. One of the interesting and promising directions of the practical application of obtained paints can be the ability for self-decontamination to finishing materials, for instance, for medical establishments and premises of public buildings, where mass public gatherings are observed.

Funding

This research was financially supported by the Polish National Science Centre, grant no. 2018/30/E/ST5/00845.

Declaration of competing interest

The authors declare that they have no known competing financial interests or personal relationships that could have appeared to influence the work reported in this paper.

References

[1] L. Morawska, W. Huang, WHO health guidelines for indoor air quality and national recommendations/standards, in: Y. Zhang, P.K. Hopke, C. Mandin (Eds.), Handbook of Indoor Air Quality, Springer, Singapore, 2022, pp. 1491–1510.

[2] A. Cincinelli, T. Martellini, Indoor air quality and health, Int. J. Environ. Res. Publ. Health 14 (11) (2017) 1–5, https://doi.org/10.3390/ijerph14111286.

[3] S. Sadrizadeh, R. Yao, F. Yuan, H. Awbi, W. Bahnfleth, Y. Bi, G. Cao, C. Croitoru, R. de Dear, F. Haghighat, P. Kumar, M. Malayeri, F. Nasiri, M. Ruud, P. Sadeghian, P. Wargocki, J. Xiong, W. Yu, B. Li, Indoor air quality and health in schools: a critical review for developing the roadmap for the future school environment, J. Build. Eng. 57 (2022) 1–23, https://doi.org/10.1016/j.jobe.2022.104908.

[4] S. Vardoulakis, E. Giagloglou, S. Steinle, A. Davis, A. Sleeuwenhoek, KS. Galea K. Dixon, J.O. Crawford, Indoor exposure to selected air pollutants in the home environment: a systematic review, Int. J. Environ. Res. Publ. Health 17 (23) (2020) 1–24, https://doi.org/10.3390/ijerph17238972.

[5] R.E. Dodson, E.A. Houseman, J. Levy, J. Spengler, J. Shine, Measured and modeled personal exposures to and risks from volatile organic compounds, Environ. Sci. Technol. 41 (2007) 8498–8505, https://doi.org/10.1021/es071127s.

[6] K. Vaali, M. Tuomela, M. Mannerström, T. Heinonen, T. Tuuminen, Toxic indoor air is a potential risk of causing immuno suppression and morbidity– a pilot study, J. Fungi 8 (2) (2022) 1–18, https://doi.org/10.3390/jof8020104.

[7] M. Wang, L. Li, C. Hou, X. Guo, H. Fu, Building and health: mapping the knowledge development of Sick Building Syndrome, Buildings 12 (3) (2022) 1–17, https://doi.org/10.3390/buildings12030287.

[8] O. Stoner, J. Lewis, I.L. Martínez, S. Gumy, T. Economou, H. Adair-Rohani, Household cooking fuel estimates at global and country level for 1990 to 2030, Nat. Commun. 12 (1) (2021) 1–8, https://doi.org/10.1038/s41467-021-26036-x.

[9] B. Gutarowska, Moulds in biodeterioration of technical materials, Folia Biol. Oecol. 10 (2014) 27–39, https://doi.org/10.2478/fobio-2014-0012.

[10] E. Gámez-Espinosa, N. Bellotti, C. Deyá, M. Cabello, Mycological studies as a tool to improve the control of building materials biodeterioration, J. Build. Eng. 32 (2020) 1–11, https://doi.org/10.1016/j.jobe.2020.101738.

[11] F. Reiß, N. Kiefer, M. Noll, S. Kalkhof, Application, release, ecotoxicological assessment of biocide in building materials and its soil microbial response, Ecotoxicol. Environ. Saf. 224 (2021) 1–14, https://doi.org/10.1016/j.ecoenv.2021.112707.

[12] N. Jones, B. Ray, K.T. Ranjit, A.C. Manna, Antibacterial activity of ZnO nanoparticle suspensions on a broad spectrum of microorganisms, FEMS Microbiol. Lett. 279 (1) (2008) 71–76, https://doi.org/10.1111/j.1574-6968.2007.01012.x.

[13] K.H. Leong, J.Q. Lee, A.A. Kumar, L.C. Sim, S. Pichiah, Facile technique for the immobilisiation of on glass substrates for applications the photocatalitic self-cleaning of indoor air pollutants, Malaysian J. Anal. Sci 23 (1) (2019) 90–99, https://doi.org/10.17576/mjas-2019-2301-11.

[14] D. Enea, M. Bellardita, P. Scalisi, G. Alaimo, L. Palmisano, Effects of weathering on the performance of self-cleaning photocatalytic paints, Cem, Concr. Compos. 96 (2019) 77–86, https://doi.org/10.1016/j.cemconcomp.2018.11.013.

[15] W. Shen, C. Zhang, Q. Li, W. Zhang, L. Cao, J. Ye, Preparation of titanium dioxide nano particle modified photocatalytic self-cleaning concrete, J. Clean. Prod. 87 (2015) 762–765, https://doi.org/10.1016/j.jclepro.2014.10.014.

[16] M. Nyden, C. Fant, Method and Use of Nanoparticles to Bind Biocides in Paints (U. S. Patent No. US 7,311,766 B2, 2007.

[17] C. Byrne, G. Subramanian, S.C. Pillai, Recent advances in photocatalysis for environmental applications, J. Environ. Chem. Eng. 6 (3) (2018) 3531–3555, https://doi.org/10.1016/j.jece.2017.07.080.

[18] J.P. Kaiser, S. Zuin, P. Wick, Is nanotechnology revolutionising the paint and lacquer industry? A critical opinion, Sci. Total Environ. 442 (2013) 282–289, https://doi.org/10.1016/j.scitotenv.2012.10.009.

[19] R. Thiruvenkatachari, S. Vigneswaran, I.S. Moon, I.S. A review on UV/TiO_2 photocatalytic oxidation process (Journal Review), Kor. J. Chem. Eng. 25 (2008) 64–72, https://doi.org/10.1007/s11814-008-0011-8.

[20] R.A.R. Monteiro, F.V.S. Lopes, A.M.T. Silva, J. Ângelo, G.V. Silva, A.M. Mendes, R. A.R. Boaventura, V.J.P. Vilar, Are TiO_2-based exterior paints useful catalysts for gas-phase photooxidation processes? A case study on n-decane abatement for air detoxification, Appl. Catal. B Environ. 147 (2014) 988–999, https://doi.org/10.1016/j.apcatb.2013.09.031.

[21] F. Salvadores, M. Reli, O.M. Alfano, K. Kočí, M.L.M. Ballari, Efficiencies evaluation of photocatalytic paints under indoor and outdoor air conditions, Front. Chem. 23 (2020) 1–13, https://doi.org/10.3389/fchem.2020.551710.

[22] M. Janus, E. Kusiak-Nejman, P. Rokicka-Konieczna, A. Markowska-Szczupak, K. Zając, A.W. Morawski, Bacterial inactivation on concrete plates loaded with modified TiO_2 Photocatalysts under visible light irradiation, Molecules 24 (17) (2019) 1–14, https://doi.org/10.3390/molecules24173026.

[23] C. George, A. Beeldens, F. Barmpas, J.-F. Doussin, G. Manganelli, H. Herrmann, J. Kleffmann, A. Mellouki, Impact of photocatalytic remediation of pollutants on urban air quality, Front. Environ. Sci. Eng. 10 (5) (2016) 1–11, https://doi.org/10.1007/s11783-016-0834-1.

[24] H. Dong, G. Zeng, L. Tang, C. Fan, C. Zhang, X. He, Y. He, An overview on limitations of TiO_2-based particles for photocatalytic degradation of organic pollutants and the corresponding countermeasures, Water Res. 1 (79) (2015) 128–146, https://doi.org/10.1016/j.watres.2015.04.038.

[25] Q. Jiang, C. Dingg, Y. Liu, A type of novel glass for indoor air cleaning under visible-light, Build. Environ. 137 (2018) 226–234, https://doi.org/10.1016/j.buildenv.2018.04.013.

[26] A. Zielińska-Jurek, I. Malinowska, Trifunctional Compound with Photocatalytic, Magnetic and Biocidal Properties Modified with Composite Particles with Non-stoichiometric Fe:Zn Content for the Production of Protective Coatings, Method of Producing This Trifunctional Composition with Photocatalytic, Magnetic and Biocidal Properties, 2021.

[27] H.B. Kamal, M.S. Antonious, M.A. Mekewi, A.M. Badawi, A.M. Gabr, K. El Baghdady, Nano ZnO/amine composites antimicrobial additives to acrylic paints, Egypt, J. Petrol. 24 (4) (2015) 397–404, https://doi.org/10.1016/j.ejpe.2015.10.005.

[28] N. Talebian, S. Matin Amininezhad, M. Doudi, Controllable synthesis of ZnO nanoparticles and their morphology-dependent antibacterial and optical properties, J. Photochem. Photobiol. B Biol. 120 (2013) 66–73, https://doi.org/10.1016/j.jphotobiol.2013.01.004.

[29] I. Malinowska, P. Madajski, A. Ostrowski, C. Gómez-Polo, L. Carvera, W. Bednarski, P. Kubica, A. Zielińska-Jurek, Synthesis, characterisation, and application of 2D/2D TiO_2-GO-$ZnFe_2O_4$ obtained by the fluorine-free lyophilisation method for solar light-driven photocatalytic degradation of ibuprofen, Environ. Sci. Pollut. Res. 30 (2023) 35929–35944, https://doi.org/10.1007/s11356-022-24587-0.

[30] ASTM E2149-01, Standard Test Method for Determining the Antimicrobial Activity of Immobilised Antimicrobial Agents under Dynamic Contact Conditions, ASTM International, West Conshohocken, PA, 2001.

[31] E.M. Mohammed, K.A. Malini, P. Kurian, M.R. Anantharaman, Modification of dielectric and mechanical properties of rubber ferrite composites containing manganese zinc ferrite, Mater. Res. Bull. 37 (2002) 753–768, https://doi.org/10.1016/S0025-5408(02)00690-6.

[32] Y. Xu, Y. Liang, L. Jiang, H. Wu, H. Zhao, D. Xue, Preparation and magnetic properties of $ZnFe_2O_4$ nanotubes, J. Nanomater. (2011) 1–5, https://doi.org/10.1155/2011/525967.

[33] M.Á. Cobos, P. de la Presa, I. Puente-Orench, I. Llorente, I. Morales, A. García-Escorial, A. Hernando, J.A. Jiménez, Coexistence of antiferro- and ferrimagnetism in the spinel $ZnFe_2O_4$ with an inversion degree δ lower than 0.3, Ceram. Int. 48 (9) (2022) 12048–12055, https://doi.org/10.1016/j.ceramint.2022.01.063.

[34] G.M. Alzoubi, The effect of Co-doping on the structural and magnetic properties of single-domain crystalline copper ferrite nanoparticles, Magnetochemistry 8 (164) (2022), https://doi.org/10.3390/magnetochemistry8120164.

[35] D.S. Mathew, R.-S. Juang, An overview of the structure and magnetism of spinel ferrite nanoparticles and their synthesis in microemulsions, J. Chem. Eng. 129 (2007) 51–65, https://doi.org/10.1016/j.cej.2006.11.001.

[36] O.M. Lemine, M. Bououdina, M. Sajieddine, A.M. Al-Saie, M. Shafi, A. Khatab, M. Al-hilali, M. Henini, Synthesis, structural, magnetic and optical properties of nanocrystalline ZnFe2O4, Phys. B. Condens. 406 (2011) 1989–1994, https://doi.org/10.1016/j.physb.2011.02.072.

[37] D. Gao, Z. Shi, Y. Xu, J. Zhang, G. Yang, J. Zhang, X. Wang, D. Xue, Synthesis, magnetic anisotropy and optical properties of preferred oriented zinc ferrite nanowire arrays, Nanoscale Res. Lett. 5 (2010) 1289–1294, https://doi.org/10.1007/s11671-010-9640-z.

[38] J. Zhou, B. Wei, M. Wang, Z. Yao, P. Chen, C. Zhou, Z. Li, Three dimensional flower like $ZnFe_2O_4$ ferrite loaded graphene: enhancing microwave absorption performance by constructing microcircuits, J. Alloys Compd. 889 (2021), https://doi.org/10.1016/j.jallcom.2021.161734.

[39] S. Latif, A. Liaqat, M. Imran, A. Javaid, N. Hussain, T. Jesionowski, M. Bilal, Development of zinc ferrite nanoparticles with enhanced photocatalytic performance for remediation of environmentally toxic pharmaceutical waste diclofenac sodium from wastewater, Environ. Res. 216 (2) (2023), https://doi.org/10.1016/j.envres.2022.114500.

[40] T. Zuccheri, M. Colonna, I. Stefanini, C. Santini, D.D. Gioia, Bactericidal activity of aqueous acrylic paint dispersion for wooden substrates based on TiO_2 nanoparticles activated by fluorescent light, Materials 6 (2013) 3270–3283, https://doi.org/10.3390/ma6083270.

[41] N. Mediouni, F. Dappozze, L. Khrouz, S. Parola, A.B.H. Amara, H.B. Rhaiem, N. Jaffrezic-Renault, P. Namour, C. Guillard, Correlation between photocatalytic properties of ZnO and generation of hydrogen peroxide-impact of composite ZnO/TiO_2 rutile and anatase, Catalysts 12 (11) (2022), https://doi.org/10.3390/catal12111445.

[42] A. Keziban, G. Nuray, Ö. Mahmut, Recent advances in photocatalytic coatings for antimicrobial surfaces, Curr. Opin. Chem. Eng. 36 (2022), https://doi.org/10.1016/j.coche.2021.100777.

[43] Y. Yan, C. Soraru, V. Keller, N. Keller, L. Ploux, Antibacterial and biofilm-preventive photocatalytic activity and mechanisms on P/F-Modified TiO_2 coatings, ACS Appl. Bio Mater. 3 (2020) 5687–5698, https://doi.org/10.1021/acsabm.0c00467.

[44] L. Hochmannova, J. Vytrasova, Photocatalytic and antimicrobial effects of interior paints, Prog. Org. Coating 67 (2010) 1–5, https://doi.org/10.1016/j.porgcoat.2009.09.016.

[45] C.R. Mendes, G. Dilarri, C.F. Forsan, Antibacterial action and target mechanisms of zinc oxide nanoparticles against bacterial pathogens, Sci. Rep. 12 (2022), https://doi.org/10.1038/s41598-022-06657-y.

[46] S. Cheeseman, A.J. Christofferson, R. Kariuki, D. Cozzolino, T. Daeneke, R. j. Crawford, V.K. Truong, J. Chapman, A. Elbourne, Antimicrobial metal nanomaterials: from passive to stimuli-activated applications, Adv. Sci. 7 (2020) 1–35, https://doi.org/10.1002/advs.201902913.

[47] S.K. Kirthika, G. Goel, A. Matthews, S. Goel, Review of the untapped potentials of antimicrobial materials in the construction sector, Prog. Mater. Sci. 133 (2023), https://doi.org/10.1016/j.pmatsci.2022.101065.

[48] E.O. Ogunsona, R. Muthuraj, E. Ojogbo, O. Valerio, T.H. Mekonnen, Engineered nanomaterials for antimicrobial applications: a review, Appl. Mater. Today 18 (2020), https://doi.org/10.1016/j.apmt.2019.10047.

[49] G.E. Yılmaz, I. Göktürk, M. Ovezova, F. Yılmaz, S. Kılıç, A. Denizli, Antimicrobial nanomaterials: a review, Hygie 3 (2023) 269–290, https://doi.org/10.3390/hygiene3030020.
[50] B.E. Sadoq, M. Britel, A. Bouajaj, R. Maalej, A. Touhami, M. Abid, H. Douiri, F. Touhami, A. Maurady, A review on antibacterial activity of nanoparticles, Biointerface Res. Appl. Chem. 13 (5) (2023) 1–19, https://doi.org/10.33263/BRIAC135.405.
[51] T. Wei, Q. Yu, H. Chen, Responsive and synergistic antibacterial coatings: fighting against bacteria in a smart and effective way, Adv. Healthcare Mater. 8 (2019) 1–24, https://doi.org/10.1002/adhm.201801381.
[52] S. Mandal, S. Natarajan, A. Tamilselvi, S. Mayadevi, Photocatalytic and antimicrobial activities of zinc ferrite nanoparticles synthesized through soft chemical route: a magnetically recyclable catalyst for water/wastewater treatment, J. Environ. Chem. Eng. 4 (3) (2016) 2706–2712, https://doi.org/10.1016/j.jece.2016.05.020.
[53] A. Garcia-Cruz, G. Rincon-Enriquez, A. Ilyina, C. Guizar-Gonzalez, Al Mtz-Enriquez, L. Diaz-Jimenez, E.E. Quinones-Aguilar, J. Enriquez-Vara, R. Ramos-Gonzalez, C.N. Aguilar-Gonzalez, Bactericidal in-vitro effect of zinc ferrite nanoparticles and the orange wax extracts on three phytopathogen microorganisms, IEEE Trans. NanoBioscience 18 (4) (2018) 528–534, https://doi.org/10.1109/TNB.2019.2937840.